Published in final edited form as:

Nature. 2011 March 17; 471(7338): 336–340. doi:10.1038/nature09731.

Crystal structure of a potassium ion transporter TrkH

Yu Cao[1,11], **Xiangshu Jin**[2,11], **Hua Huang**[1,11], **Mehabaw Getahun Derebe**[3], **Elena J. Levin**[1], **Venkataraman Kabaleeswaran**[1], **Yaping Pan**[1], **Marco Punta**[4,5], **James Love**[4], **Jun Weng**[1], **Matthias Quick**[6,7], **Sheng Ye**[3], **Brian Kloss**[4], **Renato Bruni**[4], **Erik Martinez-Hackert**[8], **Wayne A. Hendrickson**[8], **Burkhard Rost**[4,5], **Jonathan A. Javitch**[6,7,9], **Kanagalaghatta R. Rajashankar**[10], **Youxing Jiang**[3], and **Ming Zhou**[1]

[1] Department of Physiology & Cellular Biophysics, College of Physicians and Surgeons, Columbia University, 630 West 168th Street, New York, NY 10032, USA

[2] Center for Computational Biology and Bioinformatics, Department of Biochemistry and Molecular Biophysics, Howard Hughes Medical Institute, Columbia University, 1130 St. Nicholas Ave, Room 815, New York, NY 10032

[3] Department of Physiology and Howard Hughes Medical Institute, University of Texas Southwestern Medical Center, Dallas, TX 75390

[4] New York Consortium on Membrane Protein Structure, New York Structural Biology Center, 89 Convent Avenue, New York, NY 10027, USA

[5] Department of Computer Science and Institute for Advanced Study, Technical University of Munich, D-85748 Munich, Germany

[6] Center for Molecular Recognition and Department of Psychiatry, Columbia University, 630 West 168th Street, New York, NY 10032, USA

[7] New York State Psychiatric Institute, Division of Molecular Therapeutics; 1051 Riverside Drive, New York, NY 10032

[8] Department of Biochemistry and Molecular Biophysics, Howard Hughes Medical Institute, Columbia University, 630 West 168th Street, New York, NY 10032

[9] Department of Pharmacology, Columbia University, 630 West 168th Street, New York, NY 10032, USA

Correspondence and requests for materials should be addressed to M. Z. (mz2140@columbia.edu).

[11]These authors contributed equally to the work.

Author Contributions M.P., J.L., B.R. and W.A.H. identified TrkH/TrkG/KtrB homologs in the database. R.B., B.K. and J.L. cloned and tested expression of the homologs. Y.C., H.H., J.W., E.J.L. and M.Z. scaled up production of proteins, produced and refined VpTrkH crystals, and collected and analyzed X-ray diffraction data. X.J., E.J.L. and M.Z. solved and refined the structures. V.K., S.Y. and E.M-H. analysed diffraction data and obtained a partial model in early stages of the project. Y.C., M.G.D, M.Q., Y.P., Y.J., J.A.J. and M.Z. characterized VpTrkH function. K.R.R. and W.A.H. advised on data collection and crystallography. E.J.L. and M.Z wrote the manuscript with inputs from all authors.

Author information Atomic coordinates and structure factors have been deposited with the Protein Data Bank under accession ID 3PJZ.

[10] Department of Chemistry and Chemical Biology, Cornell University, NE-CAT, Advanced Photon Source, Argonne, IL 60439, USA

Abstract

The TrkH/TrkG/KtrB proteins mediate K^+ uptake in bacteria and likely evolved from simple K^+ channels by multiple gene duplications or fusions. Here we present the crystal structure of a TrkH from *Vibrio parahaemolyticus*. TrkH is a homodimer, and each protomer contains an ion permeation pathway. A selectivity filter, similar in architecture to those of K^+ channels but significantly shorter, is lined by backbone and side chain oxygen atoms. Functional studies showed that the TrkH allows permeation of K^+ and Rb^+ but not smaller ions such as Na^+ or Li^+. Immediately intracellular to the selectivity filter are an intramembrane loop and an arginine residue, both highly conserved, which constrict the permeation pathway. Substituting the arginine with an alanine significantly increases the rate of K^+ flux. These results reveal the molecular basis of K^+ selectivity and suggest a novel gating mechanism by this large and important family of membrane transport proteins.

K^+ is highly concentrated in all living cells and plays diverse physiological roles such as setting membrane potential 1, regulating turgor pressure 2 and maintaining intracellular pH 3–5. Since K^+ is virtually impermeable to the cell membrane, specialized K^+ transporters have evolved to mediate its uptake. In animal cells, K^+ uptake is mainly achieved by the Na^+-K^+-ATPase 6, while in non-animal cells, the task is shared by at least two different systems, one of which, the superfamily of K^+ transporters or the SKT proteins 7, is the focus of this research.

An SKT protein has four tandem domains with low homology to each other, each resembling a single protomer from a simple K^+-channel with a predicted M1-P-M2 transmembrane topology 8–10. M1 and M2 are transmembrane helices that are connected by P, the re-entrant pore loop, which is composed of a half-membrane spanning helix followed by an extended loop 11. In K^+ channels, the half-membrane spanning helix is called the pore helix, and the extended loop harbors the highly conserved signature sequence TVGYG, which forms the selectivity filter responsible for the coordination of K^+. In SKT proteins, the P-loops are less strictly conserved. It has been proposed that SKT proteins have a structure that resembles K^+ channels 9–10,12, and results from functional studies have been consistent with this view: mutating a conserved glycine residue in the P-loops changes ion selectivity of SKT proteins in bacteria 7,13 and plants 14; while epitope tagging of a yeast SKT protein showed that its transmembrane topology is consistent with four M1-P-M2 repeats 15.

Studies have shown that the selectivity of K^+ channels is highly sensitive to changes to the structure of the selectivity filter. Introducing point mutations to the signature sequence of K^+ channels compromises K^+ selectivity 16; and the NaK channel, which has a slightly modified signature sequence of TVGDG resulting in an altered selectivity filter conformation, is essentially non-selective between K^+ and Na^+ 17. How then can the selectivity of the SKT proteins be maintained, given that their signature sequences are so highly degraded (Fig. S1)? Furthermore, if indeed SKT proteins have the architecture of a

K^+ channel pore, how is transport of K^+ controlled? To address these questions we targeted the bacterial TrkG/TrkH/KtrB proteins, the largest subfamily of SKT proteins, for structural and functional studies. The importance of these proteins in bacteria has been shown in *Escherichia coli*, which does not grow in less than 5 mM K^+ when its *trkG* and *trkH* genes are deleted 18, and in *Francisella tularensis*, which loses its ability to cause tularaemia when lacking TrkH 19. We crystallized and solved the structure of a TrkH from *Vibrio paraheamalyticus*, hereafter VpTrkH.

Function of VpTrkH

VpTrkH was expressed and purified to homogeneity. The purified VpTrkH eluted as a single symmetrical peak on a size exclusion column (Fig. S2a), and by combining the size exclusion chromatography with light scattering and refractive index measurements, the molecular weight of the purified protein was estimated to be approximately 100 kDa. Since the molecular weight of each VpTrkH protomer is ~54 kDa, the detergent-solubilised VpTrkH is a homodimer. The homodimeric quaternary assembly was further verified by running the protein on a SDS-PAGE gel after incubation with covalent crosslinkers, which produced a band roughly twice the molecular weight (Fig. S2b). Dimeric assembly has also been reported for the KtrB protein from *Bacillus subtilis* 20–21, a protein closely related to VpTrkH.

Since VpTrkH had not been functionally characterized, we proceeded to measure its function in two experiments. First, the *VptrkH* gene was introduced into an *E. coli* strain, LB650 18, which lacks both the *trkG* and *trkH* genes. LB650 cells have a slow growth phenotype in media with less than 5 mM K^+, and expression of VpTrkH rescued the growth of these cells (Fig S2c), suggesting that VpTrkH mediates K^+ uptake. Second, purified and detergent-solubilised VpTrkH protein was reconstituted into liposomes, and K^+ permeation was measured indirectly by monitoring uptake of radioactive $^{86}Rb^+$ 17,22. In this experiment, the proteoliposomes contain a high internal concentration of K^+ and are diluted into an external solution with a low concentration of K^+ and a trace amount of radioactive $^{86}Rb^+$. Efflux of K^+ down its chemical gradient *via* VpTrkH creates an electrical potential across the bilayer that drives uptake of $^{86}Rb^+$, an ion that is known to permeate K^+ channels. Uptake of $^{86}Rb^+$ was observed only in vesicles reconstituted with VpTrkH (Fig 1a), indicating that VpTrkH is permeable to both K^+ and Rb^+. Further experiments showed that $^{86}Rb^+$ uptake is not affected by the presence of Na^+ or Li^+ in the external solution, but is inhibited by external K^+ or Rb^+ (Fig. 1b). These results indicate that despite the weak conservation of its signature sequence, VpTrkH exhibits selectivity for K^+ and Rb^+ over Na^+ and Li^+. In addition, these experiments also suggest that VpTrkH is capable of mediating facilitated diffusion of K^+ driven by an electrochemical gradient.

Overall structure

Crystals of both native and selenomethionine substituted VpTrkH were grown under oil by the microbatch method, and the best native protein crystals diffracted to 3.5 Å and belonged to the space group $P2_12_12_1$ (Table S1). Initial phases were obtained by single wavelength anomalous diffraction (SAD) 23 using a selenomethionine substituted VpTrkH crystal. The

building and refinement of the structural model were facilitated by the presence of a twofold non-crystallographic symmetry (NCS) axis and the positions of the selenium atoms. The final refined model contains residues 1–157, 174–484, and one K^+ per subunit. The region encompassing residues 158–173, which is a loop between two transmembrane helices, is disordered.

Each asymmetric unit contains a dimer of VpTrkH protomers related by a twofold symmetry axis perpendicular to the plane of the membrane. Their N- and C-termini both likely reside on the cytoplasmic side as inferred from the experimentally determined topology of a highly homologous TrkH protein from *E. coli* 24. Two views of the dimer are shown in Fig 1c & d. Viewed along the twofold axis from the extracellular side, the dimer has a parallelogram shape with sides of approximately 85 and 43 Å. Along the twofold axis vpTrkH is approximately 47 Å thick. Stereo views of the VpTrkH dimer in three orientations are shown in Fig. S3a-c.

Each VpTrkH protomer is composed of five domains, defined sequentially from the N-terminus to the C-terminus as D0 to D4 (Fig 1e, Fig S1 & S3b). D0, which is found only in the TrkH/TrkG subfamily of SKT proteins, has two transmembrane segments. D1 to D4 each have a K^+-channel-like M1-P-M2 topology, although the M2 helices of D2-4 are composed of two shorter ones (Fig 2a). The secondary structure of each P-loop also resembles that of a K^+ channel, composed of a half membrane-spanning helix, the pore helix, followed by an extended loop that forms the selectivity filter. D1 to D4 assemble around a pseudo fourfold symmetry axis to form an ion permeation pathway, and when observed from the extracellular side along the pseudo-fourfold axis, they are arranged in an anti-clockwise direction (Fig S3b). An extensive dimer interface is composed of helices from D3 and D4, with a buried surface of 2225 $Å^2$ per protomer. There is a hydrophobic cavity in the middle of the interface, but it is sealed off from the aqueous medium by two layers of hydrophobic residues on both sides of the membrane (Fig. S4). The ion permeation pathway, which is contained within each protomer, has an hourglass shape and two salient features: a selectivity filter and an intramembrane loop (Fig. 2b).

Selectivity filter

The selectivity filter is surrounded by the four pore helices, which are arranged with the negative ends of their helix-dipole moments pointing to the middle of the membrane (Fig. S5). A similar arrangement of pore helices is present in K^+ channels, and its role in minimizing the free energy of a permeating cation has been discussed for the KcsA K^+ channel 11,25.

The four selectivity filter signature sequences are located on the P-loops (Fig 3a), and these elements come together to form the selectivity filter (omit map in Fig 3b and Fig S6a, 2Fo-Fc map in Fig S6b). When compared to those of K^+ channels, the selectivity filter has a wider opening on the extracellular side and a much shorter constricted region where K^+ is coordinated (Fig. 3c-d, Fig S6c, and Fig. S7). In the constricted region, main chain and side chain oxygen atoms form stacks of oxygen rings that could coordinate and stabilize dehydrated K^+, a feature that is preserved from the K^+ channels. In a Fo-Fc map calculated

with K^+ omitted, two peaks of positive electron density appear in the filter (Fig. 3d and Fig. S7a), which we call the upper and lower site and interpret as potential positions where K^+ binds. Due to the modest resolution of the diffraction data, we cannot unambiguously determine the contribution of K^+ to these densities, as opposed to partial contribution from water molecules or calcium ions that were included in the crystallization solution. Since Rb^+ and Ba^{2+} are known to occupy K^+ positions in the selectivity filter of the KcsA K^+ channel 11,26, we took advantage of this knowledge and grew crystals in the presence of Rb^+ or Ba^{2+}. Difference electron densities corresponding to Fourier coefficients F_{Rb}-F_K or F_{Ba}-F_K are shown in Fig. 3e. In both cases, a strong positive electron density peak is present in the upper site, consistent with substitution of a K^+ with a more electron dense Rb^+ or Ba^{2+}. The upper site lines up with site 3 (S3) in the KcsA K^+ channel, and is constructed entirely by backbone carbonyl oxygen atoms (Fig. 3b and Fig. S6c). In the KcsA K^+ channels, Rb^+ does not occupy every K^+ binding site in the selectivity filer, and Rb^+ permeates with a much slower rate than K^+27–28. A slower rate of Rb^+ uptake was also observed by TrkH in *E. coli* 29. Therefore, we postulate that the lower peak in the K^+ difference map, which aligns with S4 in KcsA, could potentially be a K^+ binding site (Fig. 3d and Fig. S7), although there was no density at this location in either the Rb^+ or Ba^{2+} difference maps.

Although only one binding site has been confirmed by heavy atoms and modelled into the structure, the limited resolution of the data likely reduced our ability to observe more. Comparison to the KcsA structure suggests that the selectivity filter could potentially accommodate a maximum of three K^+ binding sites without requiring a substantial structural change. In addition to the confirmed site and the possible site corresponding to S4 in KcsA, the backbone carbonyls from the highly conserved glycine residues form a ring of oxygen atoms above the confirmed ion binding site, and could potentially form another K^+ binding site that would line up with S2 in KcsA (Fig. 3d and Fig. S7). The S1 site is lost due to the widening of the selectivity filter in TrkH. This is not wholly unexpected due to the differences in the selectivity filter sequence between TrkH and KcsA: the second glycine residue in the signature sequence of K^+ channels is not conserved in TrkH (Fig 3a), and in the high-resolution KcsA structure 30 the backbone torsion angles of this residue lie in an unfavourable region of the Ramachandran plot for non-glycine residues. Regardless of the number of sites, the structure shows that at least one dehydrated K^+ likely binds to VpTrkH through coordination by oxygen atoms in a manner similar to a K^+ channel. Further experiments are needed to measure more accurately the occupancy of K^+ and whether or not VpTrkH exhibits the high selectivity characteristic of K^+ channels. In addition, since the four-site configuration is crucial for a high K^+ throughput in K^+ channels 27,31, we conjecture that VpTrkH, if it operates by a channel-like mechanism, conducts K^+ with a lower throughput.

The ion permeation pathway

Although each protomer forms a continuous pore, a K^+ permeating from the extracellular side encounters a barrier shortly after it exits the selectivity filter (Fig. 2c). The barrier is composed of two elements: Arg468 from the second transmembrane segment of domain 4 (D4M2), and an intramembrane circular loop between D3M2a and D3M2b (Fig. 2b and Fig 4a). This is a unique feature and is not observed in any known K^+ channel structures.

Arg468 is conserved in almost all bacterial SKT proteins. The guanidinium group points towards the center of the permeation pathway and is ~3.1 Å away from the backbone carbonyl oxygen atom of Gly353, which is part of the intramembrane loop formed by Gly346 to Lys357 (Fig. 4a). This loop is present in all TrkH, TrkG and KtrB families, is rich in glycine and other small residues such as alanine and serine, and contains a number of highly conserved residues (Fig. S1 and Fig. S8). In addition, Glu470, another highly conserved residue on D4M2, is close to Lys357 in the loop and Arg360 in D3M2b: a carboxylate oxygen on Glu470 is 3.7 and 3.5 A away from the terminal nitrogens of Lys357 and Arg360, respectively. These electrostatic interactions likely further stabilize the position of the intramembrane loop (Fig. 4b and Fig. S9).

The narrow constriction formed by Arg 468 and the intramembrane loop has to widen in order for a K^+ to reach the intracellular side. To understand further the role of Arg468 in K^+ permeation, we substituted it with an alanine and reconstituted the R468A mutant protein into liposomes. $^{86}Rb^+$ flux was then measured for both the wild type and the R468A mutant in side-by-side experiments. Tracer uptake by the R468A mutant is significantly faster than that by the wild type (Fig. 4c), consistent with the observation that R468 occludes K^+ permeation. An earlier study showed that mutating the equivalent of Arg468 in a KtrB reduces K^+ uptake in *E. coli* 32, seeming to contradict our functional results and the role of Arg468 inferred from the structure. However, since the KrtB mutant was assayed *in vivo*, additional factors such expression levels or association with auxiliary proteins could have affected the measurement. As for the role of the intramembrane loop, a recent study showed that various deletions of the corresponding loop in a KtrB significantly increase K^+ transport activity 33, consistent with its position shown in the structure.

Discussion

The pseudo-symmetry arising from duplication of an ancestral channel that is observed in the SKT family is not unique among ion channel/transporter families. In the animal kingdom, gene fusion or duplication of a more complex potassium channel, the voltage-dependent K^+ channel (K_v), generated voltage-dependent Na^+ and Ca^{2+} channels (Na_v and Ca_v, respectively) 34–35. Similar to the SKT proteins, four pseudo-subunits of K_v channels are expressed as a single polypeptide chain in the Na_v and Ca_v channels, although the domains are assembled in a clockwise direction when viewed from the extracellular side 36–37 in contrast to the counter-clockwise orientation observed in VpTrkH. The pseudo fourfold symmetry in VpTrkH is strongest at the ion binding sites in the selectivity filter region, where each domain contributes similarly to coordination of a K^+. However, the symmetry starts to break down outside of the selectivity filter where the pore helices vary in length and form different angles with the membrane norm, and the symmetry becomes considerably weaker for the M1 and M2 helices from different homologous domains. Especially notable is D3, which contains the intramembrane loop and the tilted D3M2b helix, and therefore is expected to contribute to gating of the permeation pathway more than the other domains. It is likely that in Nav and Cav channels, the fourfold symmetry is maintained at the selectivity region for coordination of permeating ions but gradually breaks down so that the voltage-sensing modules and the connected gating machinery of a particular pseudo-subunit may contribute more than the other ones.

TrkH/TrkG and KtrB assemble with the cytosolic adenine nucleotide-binding proteins TrkA 38–39 and KtrA 40, respectively. KtrA forms a ring and can undergo significant conformational changes upon binding to or changes in the oxidation state of ligands such as NAD and ATP 20,41–42. The ring has a twofold symmetry that matches that of the homo-dimeric assembly of the transmembrane subunits, and could potentially allosterically control K^+ permeation. We speculate that the dimeric assembly is required for regulation of K^+ transport by TrkA, although each monomer contains an independent ion permeation pathway. Although the structure of VpTrkH alone does not offer a clear answer as to whether TrkH operates as a channel or a transporter, it provides a framework for further studies that will reveal the molecular mechanism of K^+ uptake and its regulation by intracellular TrkA subunit.

Methods Summary

Both native and selenomethionine-substituted VpTrkH were expressed in *E. coli* with a C-terminal polyhistidine tag, extracted into decylmaltoside, and purified by a metal affinity column. The proteins were further purified by size-exclusion chromatography and concentrated to 8–10 mg/mL for crystallization trials. Crystals were obtained by microbatch crystallization under paraffin oil. Co-crystallization with different ions was achieved by running the size-exclusion chromatography in buffers containing 150 mM of KCl, RbCl, or $BaCl_2$. Initial phases were obtained by SAD from a 3.9 Å dataset collected on selenomethionine-derivatized VpTrkH, and a 3.5 Å native dataset (with K^+) was used for refinement of the final model. The final R and R_{free} values were 24.9 and 29.9%, respectively. Purified VpTrkH was reconstituted into liposomes for $^{86}Rb^+$ flux assays as described previously 22.

Full Methods

Homology screen, cloning and initial protein expression

TrkH was first established to be a valid target for structural studies by a bioinformatics analysis 43–44. A total of 91 *trkG*/*trkH*/*ktrB* genes from 58 prokaryotic genomes were identified, and the genes were amplified by PCR from the genomic DNAs, inserted into a modified pET plasmid (Novagen) with a C-terminal deca-histidine tag and a TEV protease recognition site, and expressed in a small-scale culture. Protein expression was then examined using Western blots as a readout, and Western-positive clones were pursued for further study. Identification and cloning of homologs, and the initial expression study were performed by a high throughput approach in the central facility of the New York Consortium on Membrane Protein Structure (NYCOMPS), and a detailed description of the procedures can be found in ref 43.

Large-scale protein expression, purification and crystallization

Western-positive clones received from the NYCOMPS were scaled up for mid- to large-scale expression studies. Five proteins (TrkHs from *Vibrio parahaemolyticus*, *Vibrio fischeri*, *Idiomarina loihiensis*, *Campylobacter jejuni* and a KtrB from *Vibrio fischeri*) had yields higher than 0.25 mg/liter cell culture and 3 of them (TrkHs from *Vibrio parahaemolyticus*, *Idiomarina loihiensis* and *Campylobacter jejuni*) exhibited a mono-

dispersed profile in size exclusion chromatography. Among those proteins, only TrkH from *Vibrio parahaemolyticus* (VpTrkH) produced diffracting crystals and thus became the focus of crystallization efforts.

For large-scale purification of native VpTrkH, BL21(DE3) cells were grown in Luria broth at 37°C and induced with 0.5 mM isopropyl β-D-1-thiogalactopyranoside (IPTG) after OD_{600nm} reached 1.0; for expression of selenomethionine incorporated proteins, the cells were grown in minimal medium containing 32.2 mM K_2HPO_4, 11.7 mM KH_2PO_4, 6 mM $(NH_4)_2SO_4$, 0.68 mM Na Citrate, 0.17 mM Mg_2SO_4, 32 mM glucose, 0.008% (w/v) alanine, arginine, aspartic acid, asparagine, cysteine, glutamic acid, glycine, histidine, proline, serine, tryptophan, glutamine and tyrosine, 0.02% (w/v) isoleucine, leucine, lysine, phenylalanine, threonine and valine, 25 mg/L L-selenium-methionine, 32 mg/L thiamine, 32 mg/L thymine) and induced at an OD_{600nm} of 0.6. The cell membranes were solubilised with 40 mM *n*-decyl-β-D-maltoside (Anatrace) and the His-tagged protein was purified with TALON Metal Affinity Resin (Clontech Inc.). After removal of the tag with tobacco etch virus protease, the native protein was subjected to size exclusion chromatography with a Superdex 200 10/300 GL column (GE Health Sciences) pre-equalized in a buffer of 150 mM KCl, 20 mM HEPES, pH 7.5, 5 mM β-mercaptoethanol and 3.5 mM *n*-decyl-β-D-maltoside. The selenomethionine-incorporated vpTrkH protein was purified by the same procedure. The native protein was concentrated to 8 mg/ml and the selenomethionine-substituted protein to 10mg/ml as approximated by ultraviolet absorbance.

Although both the native and selenomethionine-substituted VpTrkH yielded crystals readily, the crystals diffracted anisotropically and an overwhelming majority failed to reach 4.0 Å. More than 3000 crystals were screened over a period of over three years. Native VpTrkH crystals were grown by microbatch crystallization under paraffin oil where 1.5 μl of the protein solution was mixed with an equal volume of crystallization solution containing 35% PEG400, 200 mM calcium acetate and 100 mM sodium acetate, pH 5.3. Rb^+-derivatized crystals were obtained by the same method except that the size exclusion chromatography during purification was conducted in a buffer using 150 mM RbCl to replace KCl. Ba^{2+}-derivatized crystals were obtained by adding 10 mM $BaCl_2$ into the native protein prior to mixing with crystallization solution. Before flash-freezing in liquid nitrogen, the crystals were cryoprotected in mother liquor for 2–5 seconds. The mother liquor was obtained by vapor diffusion in sitting-drops mixed from 3 μl of the protein solution and an equal volume of well solution containing 35% PEG400, 200 mM calcium acetate and 100 mM sodium acetate, pH 5.3.

Data collection and structure solution

Diffraction data were collected on beamlines X25 and X29 at the National Synchrotron Light Source and 24ID-C and 24ID-E at the Advanced Photon Source. A 3.9 A dataset was collected at a wavelength of 0.9791 Å on selenomethionine-derivatized vpTrkH. The data were indexed, integrated and scaled using HKL2000 45. The dataset showed anisotropy, but nonetheless exhibited a strong anomalous signal and was therefore used to obtain the initial phases to 3.9 Å by the SAD method. The positions of 18 out of 24 available selenium sites in the asymmetric unit were located using the program phenix.hyss 46. Initial experimental

phases were improved by twofold NCS averaging and solvent flattening using RESOLVE 46. The resultant density-modified experimental map was used to manually build a partial Cαtrace with COOT 47. The phases were gradually extended to a higher resolution native dataset at 3.5 Å using twofold NCS averaging, solvent flattening, and histogram matching in DM 48. Manual model building and sequence assignments were done iteratively using COOT, and the structure refinement was done using PHENIX 46 with strong twofold NCS restraints. The final refined model contains residues 1–157, 174–484, and one K^+ in each subunit in the asymmetric unit. The anomalous difference Fourier map calculated with phases from the refined model confirmed the correctness of the initial selenium sites, all of which overlay well with ordered methionine residues in the final model, and identified two additional sites corresponding to two N-terminal methionines in the asymmetric unit (Fig S10a-b). The region encompassing residues 158–173 is disordered, consistent with the absence of anomalous peaks expected from Met158 and Met174 within this region. At the model building stage, diffraction data were corrected for anisotropy using the Anisotropy Server 49 and a second model was refined with anisotropy correction. Models with or without the correction essentially overlap, however, map quality is improved in several regions after the correction.

The final refined model devoid of K^+ was used to calculate the F_{Rb}-F_K and F_{Ba}-F_K difference maps for structures containing Rb^+ and Ba^{2+}.

E. coli complementation assay

E. coli strain LB650 competent cells were transformed with pET31 vector carrying *V. parahaemolyticus trkH*. Two media, Hi-K and Lo-K, were prepared based on ref 50, and both contain 8 mM ammonium sulfate, 0.4 mM magnesium sulfate, 1 mM sodium citrate, 1 mg/L thiamine, and 2 g/L glucose. For the Hi-K medium, 115 mM potassium phosphate (pH 7.0) was added and for the Lo-K medium 115 mM sodium phosphate (pH 7.0) was added. The two solutions were mixed in different ratios to produce the desired K^+ concentration. The transformation cell culture was spread onto agar plates prepared with solutions with different K^+ concentrations and incubated at 37°C overnight. As a blank control, pET31 vector without insertions was used to transform *E. coli* strain LB650 competent cells.

Reconstitution of TrkH into proteoliposomes

Purified VpTrkH was reconstituted into lipid vesicles composed of 1-palmitoyl-2-oleoyl-phosphatidylethanolamine and 1-palmitoyl-2-oleoyl-phosphatidylglycerol (Avanti Polar Lipids) in a ratio of 3:1 by weight, as previously described 31. The protein to lipid ratio is 1:150 by weight. The solution was then subjected to several rounds of dialysis against reconstitution solution until the detergent was totally removed. At the end of each experiment, valinomycin was added to the reaction mixture to monitor the maximum uptake.

Determination of protein oligomeric state

The mass of the VpTrkH protein in solution was measured using a Wyatt miniDAWN TREOS 3 angle-static light-scattering detector, a Wyatt Optilab rEX refractive index detector and an Agilent variable wavelength detector UV absorbance detector51. Purified protein sample (5 μl) was injected onto a TSK-GEL SuperSW3000 (4.6 mm ID by 30 cm)

silica-gel size-exclusion column in buffer containing 0.016% of dodecylmaltoside at a rate of 0.25 ml min^{-1}. The differential refractive index (dn/dc) value for DDM was calculated to be 0.128 ml g^{-1} using the Wyatt Optilab rEX refractive index detector. Deconvolution of the protein detergent conjugate was then achieved using a previously described method 52. The calculation did not account for refractive index contributions due to bound lipid.

^{86}Rb flux assay

The $^{86}Rb^+$ flux assay was performed as described previously22. In the competition assays, Li^+, Na^+, K^+, or Rb^+ were added directly into the flux buffer, and the readings were taken at the 20 minute time point.

Supplementary Material

Refer to Web version on PubMed Central for supplementary material.

Acknowledgments

Data for this study were measured at beamlines X4A, X4C, X25, and X29 of the National Synchrotron Light Source and the NE-CAT 24ID-C and E at the Advanced Photon Source. This work was supported by the US National Institutes of Health (HL086392, DK088057, and GM05026-sub0007 to M.Z.) and the American Heart Association (0630148N to M.Z.). M.Z is a Pew Scholar in Biomedical Sciences. The NYCOMPS central facility is supported by GM05026 to W.A.H. as part of the Protein Structure Initiative (PSI-2) established by the National Institute of General Medical Sciences. We thank Dr. B. Honig for support, Dr. Kirsten Jung for providing *E. coli* LB650, and Drs. J. Morais-Cabral, S-Y Lee, H. R. Guy, C. L. Slayman, and E. P. Bakker for discussions and comments on the manuscript. M.Z. is grateful to Dr. R. MacKinnon for advice and support throughout the project.

References

1. Hille, B. Ion channels of excitable membranes. 3. Sinauer; 2001.
2. Schultz SG, Epstein W, Solomon AK. Cation Transport in *Escherichia coli*. IV. Kinetics of Net K Uptake. J Gen Physiol. 1963; 47:329–346. [PubMed: 14080819]
3. Kroll RG, Booth IR. The role of potassium transport in the generation of a pH gradient in Escherichia coli. Biochem J. 1981; 198:691–698. [PubMed: 7034732]
4. Plack RH Jr, Rosen BP. Cation/proton antiport systems in *Escherichia coli*. Absence of potassium/proton antiporter activity in a pH-sensitive mutant. J Biol Chem. 1980; 255:3824–3825. [PubMed: 6989828]
5. Bakker EP, Mangerich WE. Interconversion of components of the bacterial proton motive force by electrogenic potassium transport. J Bacteriol. 1981; 147:820–826. [PubMed: 6268609]
6. Skou JC. The influence of some cations on an adenosine triphosphatase from peripheral nerves. Biochim Biophys Acta. 1957; 23:394–401. [PubMed: 13412736]
7. Tholema N, et al. All four putative selectivity filter glycine residues in KtrB are essential for high affinity and selective K^+ uptake by the KtrAB system from *Vibrio alginolyticus*. J Biol Chem. 2005; 280:41146–41154. [PubMed: 16210320]
8. Jan LY, Jan YN. Cloned potassium channels from eukaryotes and prokaryotes. Annu Rev Neurosci. 1997; 20:91–123. [PubMed: 9056709]
9. Durell SR, Hao Y, Nakamura T, Bakker EP, Guy HR. Evolutionary relationship between K^+ channels and symporters. Biophys J. 1999; 77:775–788. [PubMed: 10423425]
10. Durell SR, Guy HR. Structural models of the KtrB, TrkH, and Trk1,2 symporters based on the structure of the KcsA K^+ channel. Biophys J. 1999; 77:789–807. [PubMed: 10423426]
11. Doyle DA, et al. The structure of the potassium channel: molecular basis of K^+ conduction and selectivity. Science. 1998; 280:69–77. [PubMed: 9525859]

12. Durell SR, Bakker EP, Guy HR. Does the KdpA subunit from the high affinity K^+-translocating P-type KDP-ATPase have a structure similar to that of K^+ channels? Biophys J. 2000; 78:188–199. [PubMed: 10620285]
13. Tholema N, Bakker EP, Suzuki A, Nakamura T. Change to alanine of one out of four selectivity filter glycines in KtrB causes a two orders of magnitude decrease in the affinities for both K^+ and Na^+ of the Na^+ dependent K^+ uptake system KtrAB from *Vibrio alginolyticus*. FEBS Lett. 1999; 450:217–220. [PubMed: 10359077]
14. Maser P, et al. Glycine residues in potassium channel-like selectivity filters determine potassium selectivity in four-loop-per-subunit HKT transporters from plants. Proc Natl Acad Sci U S A. 2002; 99:6428–6433. [PubMed: 11959905]
15. Zeng GF, Pypaert M, Slayman CL. Epitope tagging of the yeast K^+ carrier Trk2p demonstrates folding that is consistent with a channel-like structure. J Biol Chem. 2004; 279:3003–3013. [PubMed: 14570869]
16. Heginbotham L, Lu Z, Abramson T, MacKinnon R. Mutations in the K^+ channel signature sequence. Biophys J. 1994; 66:1061–1067. [PubMed: 8038378]
17. Shi N, Ye S, Alam A, Chen L, Jiang Y. Atomic structure of a Na^+- and K^+-conducting channel. Nature. 2006; 440:570–574. [PubMed: 16467789]
18. Stumpe S, Bakker EP. Requirement of a large K^+-uptake capacity and of extracytoplasmic protease activity for protamine resistance of *Escherichia coli*. Arch Microbiol. 1997; 167:126–136.
19. Alkhuder K, Meibom KL, Dubail I, Dupuis M, Charbit A. Identification of *trkH*, encoding a potassium uptake protein required for *Francisella tularensis* systemic dissemination in mice. PLoS One. 2010; 5:e8966. [PubMed: 20126460]
20. Albright RA, Ibar JL, Kim CU, Gruner SM, Morais-Cabral JH. The RCK domain of the KtrAB K^+ transporter: multiple conformations of an octameric ring. Cell. 2006; 126:1147–1159. [PubMed: 16990138]
21. Albright RA, Joh K, Morais-Cabral JH. Probing the structure of the dimeric KtrB membrane protein. J Biol Chem. 2007; 282:35046–35055. [PubMed: 17932047]
22. Heginbotham L, Kolmakova-Partensky L, Miller C. Functional reconstitution of a prokaryotic K^+ channel. J Gen Physiol. 1998; 111:741–749. [PubMed: 9607934]
23. Hendrickson WA. Determination of macromolecular structures from anomalous diffraction of synchrotron radiation. Science. 1991; 254:51–58. [PubMed: 1925561]
24. Daley DO, et al. Global topology analysis of the *Escherichia coli* inner membrane proteome. Science. 2005; 308:1321–1323. [PubMed: 15919996]
25. Roux B, MacKinnon R. The cavity and pore helices in the KcsA K^+ channel: electrostatic stabilization of monovalent cations. Science. 1999; 285:100–102. [PubMed: 10390357]
26. Lockless SW, Zhou M, MacKinnon R. Structural and thermodynamic properties of selective ion binding in a K^+ channel. PLoS Biol. 2007; 5:e121. [PubMed: 17472437]
27. Morais-Cabral JH, Zhou Y, MacKinnon R. Energetic optimization of ion conduction rate by the K^+ selectivity filter. Nature. 2001; 414:37–42. [PubMed: 11689935]
28. LeMasurier M, Heginbotham L, Miller C. KcsA: it's a potassium channel. J Gen Physiol. 2001; 118:303–314. [PubMed: 11524460]
29. Schlosser A, Meldorf M, Stumpe S, Bakker EP, Epstein W. TrkH and its homolog, TrkG, determine the specificity and kinetics of cation transport by the Trk system of *Escherichia coli*. J Bacteriol. 1995; 177:1908–1910. [PubMed: 7896723]
30. Zhou Y, Morais-Cabral JH, Kaufman A, MacKinnon R. Chemistry of ion coordination and hydration revealed by a K^+ channel-Fab complex at 2.0 A resolution. Nature. 2001; 414:43–48. [PubMed: 11689936]
31. Zhou M, MacKinnon R. A mutant KcsA K^+ channel with altered conduction properties and selectivity filter ion distribution. J Mol Biol. 2004; 338:839–846. [PubMed: 15099749]
32. Kato N, et al. Role of positively charged amino acids in the $M2_D$ transmembrane helix of Ktr/Trk/HKT type cation transporters. Channels (Austin). 2007; 1:161–171. [PubMed: 18690031]
33. Hanelt I, et al. Gain of function mutations in membrane region M_{2C2} of KtrB open a gate controlling K^+ transport by the KtrAB system from *Vibrio alginolyticus*. J Biol Chem. 2010; 285:10318–10327. [PubMed: 20097755]

34. Noda M, et al. Primary structure of Electrophorus electricus sodium channel deduced from cDNA sequence. Nature. 1984; 312:121–127. [PubMed: 6209577]
35. Mikami A, et al. Primary structure and functional expression of the cardiac dihydropyridine-sensitive calcium channel. Nature. 1989; 340:230–233. [PubMed: 2474130]
36. Li RA, et al. Clockwise domain arrangement of the sodium channel revealed by μ-conotoxin (GIIIA) docking orientation. J Biol Chem. 2001; 276:11072–11077. [PubMed: 11154701]
37. Stary A, Shafrir Y, Hering S, Wolschann P, Guy HR. Structural model of the $Ca_V1.2$ pore. Channels (Austin). 2008; 2:210–215. [PubMed: 18836302]
38. Bossemeyer D, et al. K^+-transport protein TrkA of *Escherichia coli* is a peripheral membrane protein that requires other *trk* gene products for attachment to the cytoplasmic membrane. J Biol Chem. 1989; 264:16403–16410. [PubMed: 2674131]
39. Schlosser A, Hamann A, Bossemeyer D, Schneider E, Bakker EP. NAD^+ binding to the Escherichia coli K^+-uptake protein TrkA and sequence similarity between TrkA and domains of a family of dehydrogenases suggest a role for NAD^+ in bacterial transport. Mol Microbiol. 1993; 9:533–543. [PubMed: 8412700]
40. Nakamura T, Yuda R, Unemoto T, Bakker EP. KtrAB, a new type of bacterial K^+-uptake system from *Vibrio alginolyticus*. J Bacteriol. 1998; 180:3491–3494. [PubMed: 9642210]
41. Roosild TP, Miller S, Booth IR, Choe S. A mechanism of regulating transmembrane potassium flux through a ligand-mediated conformational switch. Cell. 2002; 109:781–791. [PubMed: 12086676]
42. Roosild TP, et al. KTN (RCK) domains regulate K^+ channels and transporters by controlling the dimer-hinge conformation. Structure. 2009; 17:893–903. [PubMed: 19523906]
43. Love J, et al. The New York Consortium on Membrane Protein Structure (NYCOMPS): a high-throughput platform for structural genomics of integral membrane proteins. J Struct Funct Genomics. 2010; 11:191–199. [PubMed: 20690043]
44. Punta M, et al. Structural genomics target selection for the New York consortium on membrane protein structure. J Struct Funct Genomics. 2009; 10:255–268. [PubMed: 19859826]
45. Otwinowski Z, Minor W. Processing of X-ray Diffraction Data Collected in Oscillation Mode. Methods in Enzymology. 1997; 276:307–326.
46. Adams PD, et al. PHENIX: a comprehensive Python-based system for macromolecular structure solution. Acta Crystallogr D Biol Crystallogr. 2010; 66:213–221. [PubMed: 20124702]
47. Emsley P, Cowtan K. Coot: model-building tools for molecular graphics. Acta Crystallogr D Biol Crystallogr. 2004; 60:2126–2132. [PubMed: 15572765]
48. Cowtan K. Error estimation and bias correction in phase-improvement calculations. Acta Crystallogr D Biol Crystallogr. 1999; 55:1555–1567. [PubMed: 10489450]
49. Strong M, et al. Toward the structural genomics of complexes: crystal structure of a PE/PPE protein complex from Mycobacterium tuberculosis. Proc Natl Acad Sci U S A. 2006; 103:8060–8065. [PubMed: 16690741]
50. Epstein W, Kim BS. Potassium transport loci in *Escherichia coli* K-12. J Bacteriol. 1971; 108:639–644. [PubMed: 4942756]
51. Slotboom DJ, Duurkens RH, Olieman K, Erkens GB. Static light scattering to characterize membrane proteins in detergent solution. Methods. 2008; 46:73–82. [PubMed: 18625320]
52. Kendrick BS, Kerwin BA, Chang BS, Philo JS. Online size-exclusion high-performance liquid chromatography light scattering and differential refractometry methods to determine degree of polymer conjugation to proteins and protein-protein or protein-ligand association states. Anal Biochem. 2001; 299:136–146. [PubMed: 11730335]
53. Ho BK, Gruswitz F. HOLLOW: generating accurate representations of channel and interior surfaces in molecular structures. BMC Struct Biol. 2008; 8:49. [PubMed: 19014592]

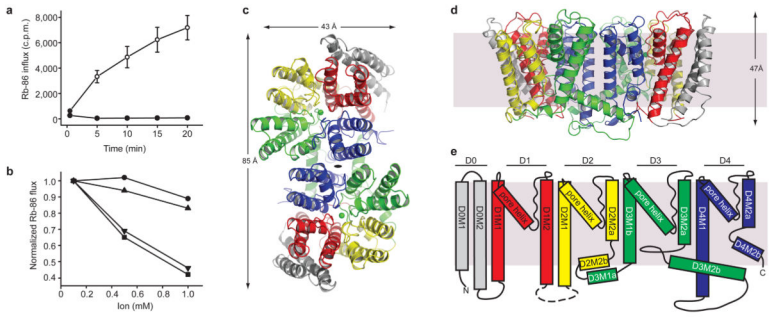

Figure 1. Function and structure of VpTrkH

(a) Time-dependent ^{86}Rb influx into liposomes reconstituted with VpTrkH (open circle) or empty vesicles (solid circle). **(b)** ^{86}Rb influx at 20 minutes in the presence of three concentrations of K^+ (square), Rb^+ (inverted triangle), Na^+ (circle), and Li^+ (triangle). **(c)** Stereo view of the VpTrkH dimer colored by domain and viewed from the extracellular side. The twofold symmetry axis is marked as a black oval. The green spheres are K^+ atoms. **(d)** VpTrkH viewed from within the membrane with the extracellular side on top. The dimer is rotated by 90° about the x- and y- axes relative to **a**. Gray rectangle representing the membrane is shown with a thickness of 30 Å. **(e)** VpTrkH topology shown with the extracellular side on top. The five domains are colored according to the same scheme as in the previous panels. The gray rectangle indicates the thickness of the cell membrane, and the unresolved loop is shown as a dotted line.

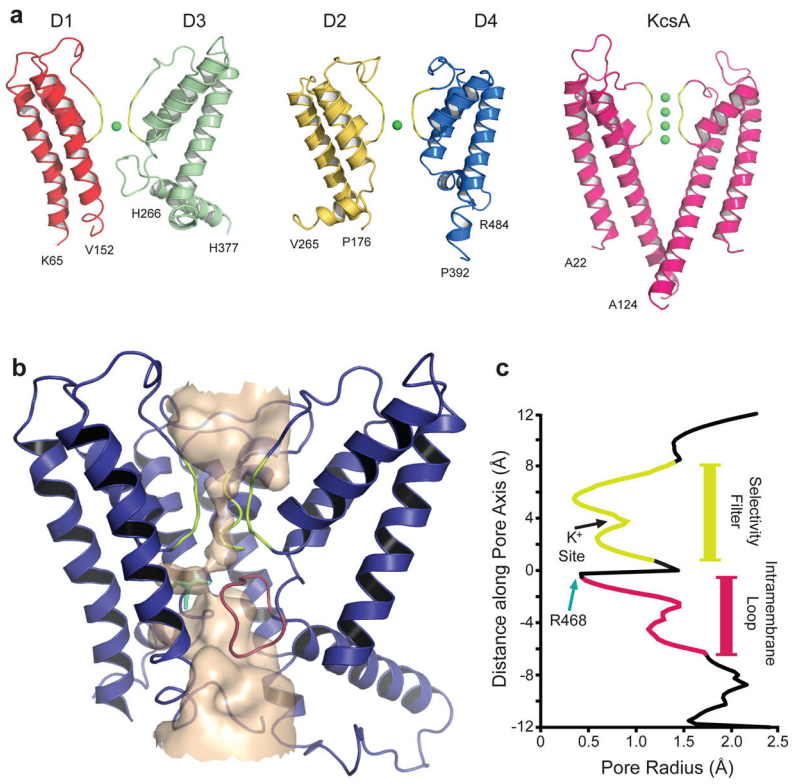

Figure 2. The VpTrkH pore

(a) Views of a VpTrkH protomer showing only the D1 and D3 domains (left) or the D2 and D4 domains (middle). Two domains of KcsA are shown on the right for comparison. K^+ atoms are shown as green spheres, and the N- and C-terminal residues are labelled. **(b)** Surface representation of the pore of a TrkH subunit obtained with the program Hollow 53 using a 1.4 Å probe radius for the vestibules and a 0.75 Å probe radius for the constricted region. The protein is shown with domain 2 removed for clarity and the selectivity filter (yellow), the intramembrane loop (magenta) and residue R468 (teal) highlighted. **(c)** Radius of the pore calculated with the program HOLE.

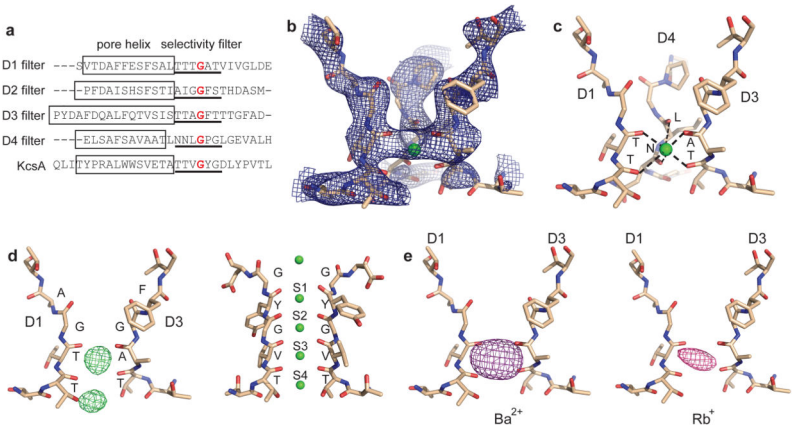

Figure 3. Selectivity filter of VpTrkH

(a) Amino acid sequence alignment of the selectivity filter regions (underlined) and pore helices (box) in VpTrkH with the selectivity filter of the KcsA K+ channel. The highly conserved glycine residue is marked in red. **(b–c)** The selectivity filter with domain 2 removed, shown with **(b)** an NCS-averaged, simulated annealing omit map calculated with six residues from each selectivity filter omitted, contoured at 1 σ, or **(c)** the coordination geometry of the K^+ (green sphere) highlighted. **(d)** D1 and D3 from the K^+ structure are shown with Fo-Fc electron density calculated without K^+ in the model and contoured at 3.5 σ. The filter of KcsA is shown on the right for comparison. **(d)** Ion binding sites in the selectivity filter. Ba^{2+} (left) and Rb^+ (right) [Fo(ion) − Fo(K^+)] difference Fourier maps are shown contoured at 6.0 and 3.5 σ levels, respectively, calculated using phases from the K^+ structure. The stick models are D1 and D3 from the K^+ structure.

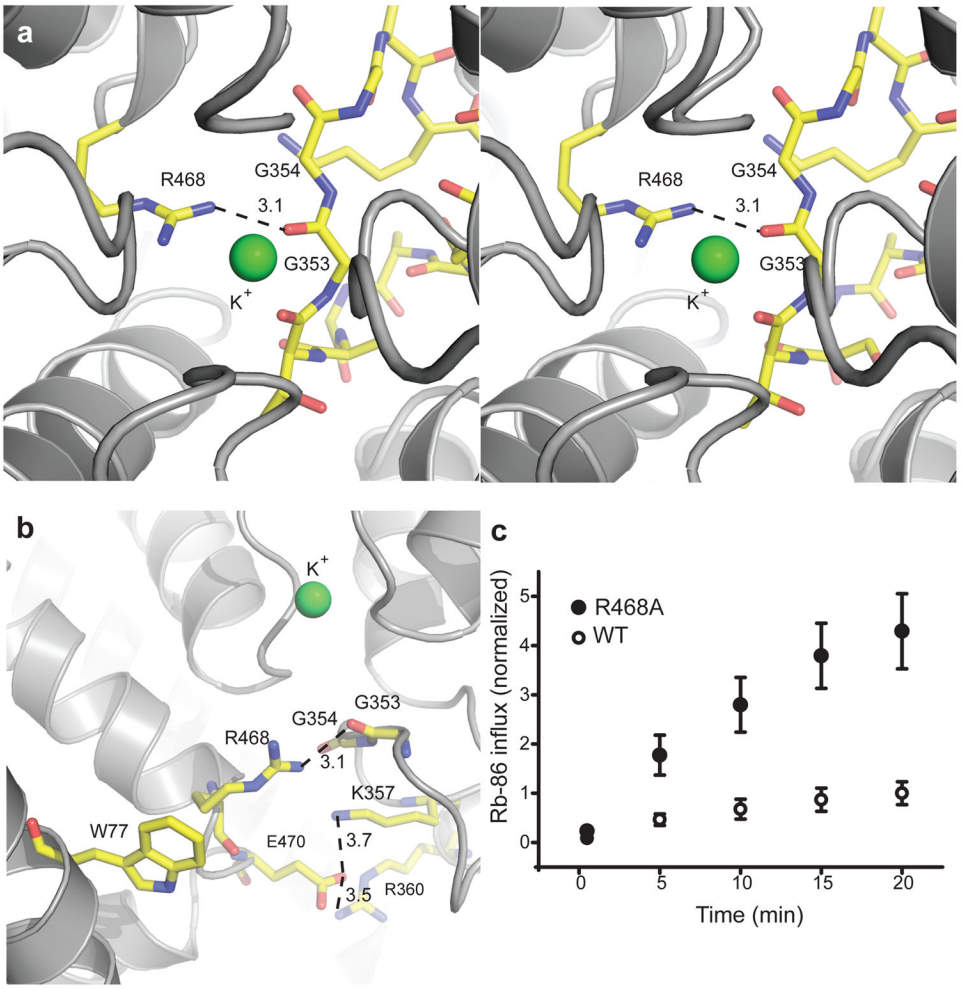

Figure 4. Constriction formed by Arg 468 and the intramembrane loop

(a) Stereo view of the interactions between the intramembrane loop and Arg468 as viewed looking down the selectivity filter from the extracellular side. **(b)** Stereo view of interactions between the intramembrane loop and Arg468 and Glu470 as viewed from within the plane of the membrane. Residues Gly353-354, Lys357, Arg360, Arg468 and Glu470 are shown as stick representations and the dashed lines indicate distances between them. **(c)** Time-dependent ^{86}Rb influx into proteoliposomes reconstituted with WT (open circle) or R468A (solid circle) VpTrkH. The error bars correspond to the S.E.M.